Effect of $\mathbf{E} \times \mathbf{B}$ driven transport on the deposition of carbon in the outer divertor of ASDEX Upgrade

L. Aho-Mantila[a,b]*, M. Wischmeier[c], K. Krieger[c], V. Rohde[c], H.W. Müller[c], D.P. Coster[c], M. Groth[b], A. Kirschner[d], R. Neu[c], S. Potzel[c], B. Sieglin[c], E. Wolfrum[c] and the ASDEX Upgrade Team

[a]*VTT Technical Research Centre of Finland, FI-02044 VTT, Finland*

[b]*Aalto University, FI-02015 TKK, Finland*

[c]*Max-Planck Institut für Plasmaphysik, D-85748 Garching, Germany*

[d]*Forschungszentrum Jülich, Trilateral Euregio Cluster, D-52425 Jülich, Germany*

Abstract

Reversal of the toroidal magnetic field and plasma current is observed to considerably change the re-deposition of ^{13}C injected into the outer divertor scrape-off layer of ASDEX Upgrade. In forward field low-density L-mode plasmas, 24-32% of injected carbon is found locally re-deposited. The deposition tails are aligned toroidally both upstream and downstream of the exit holes and indicate transport towards the strike point. In reversed field with similar main plasma parameters, the re-deposition efficiency is a factor of 2 smaller. The deposition is more localized and shows transport towards the outer scrape-off layer. Numerical modelling with the SOLPS5.0 and ERO codes shows that these differences in ^{13}C deposition can be attributed to the combination of the $\mathbf{E} \times \mathbf{B}$ drift reversal directly influencing the transport of carbon and changes in local plasma conditions due to the drift reversal.

PACS: 52.25.Fi, 52.25.Vy, 52.30.Ex, 52.40.Hf, 52.55.Rk, 52.65.Pp

JNM keywords: C0100, D0500, I0100, R0900, T0100

PSI-19 keywords: Carbon impurities, Particle Drifts, ASDEX-Upgrade, B2/EIRENE, ERO-TEXTOR

**Corresponding author address:* P.O. Box 1000, FI-02015 VTT

**Corresponding author E-mail:* leena.aho-mantila@vtt.fi

Presenting author: Leena Aho-Mantila

Presenting author E-mail: leena.aho-mantila@vtt.fi

1 Introduction

Due to its good thermal properties, carbon is one of the key materials considered for the plasma-facing components in future fusion reactors. However, its use even on restricted areas such as the divertor targets may be prohibited during burning plasma operation, due to the co-deposition of tritium and the long-range migration associated with eroded carbon. To predict transport and deposition of carbon in future machines, it is crucial to understand the observations made in present devices, and to validate the relevant numerical tools against existing experimental data.

This paper presents experimental results on carbon deposition in the tungsten-coated vertical outer target of ASDEX Upgrade (AUG) during low-confinement mode (L-mode) plasma discharges in forward and reversed magnetic field configuration. The experiments are simulated with the SOLPS5.0 and ERO codes, emphasizing on the effect of cross-field drifts on the resulting deposition pattern. The work presents the first quantitative comparison between modelled and measured carbon deposition in these experiments. It also presents the first comparison between SOLPS5.0 simulations and Langmuir probe measurements in AUG reversed field plasmas.

2 Experimental

Carbon transport in the AUG lower outer divertor has been investigated by injecting $^{13}CH_4$ from two poloidally separated valves into the SOL in repetitions of identical plasma discharges, followed by a prompt removal of the relevant tiles for post-mortem analysis of ^{13}C deposition. This paper focuses on experiments with low-density, lower-single-null L-mode plasmas, carried out at the end of the 2007 and 2009 experimental campaigns in forward and reversed magnetic field configurations, respectively.

In forward field (ion ∇B drift towards the lower divertor), $^{13}CH_4$ was injected during 11 successive discharges (#22573-75, #22577-81, #22583-85) with I_{p}=+800kA and B_{T}=-2.5T. The discharges had 0.75 MW ECRH heating and the line-averaged density was $\overline{n}_{\mathrm{e}}$=3.2$\times 10^{19}$m^{-3} (34% of the Greenwald density, n_{GW}). The outer target was in the attached, low-recycling regime, with peak temperature $T_t \sim 25$ eV and density $n_t \sim 6 \times 10^{18}$ m^{-3}, see Figure 1. The

total injection time of $^{13}CH_4$ was 33 s, comprising 80% of the total flattop time. 12% of the injection time was under Ohmic conditions. For further details, see [1, 2].

In reversed field, $^{13}CH_4$ was injected into 8 discharges (#25883-90) with $I_{\rm p}$=-800kA and $B_{\rm T}$=+2.5T, having line-averaged density $\overline{n}_{\rm e}$=3.4$\times 10^{19}$m^{-3} (0.32$n_{\rm GW}$) and 0.90 MW ECRH heating. As in forward field, the outer target remained in the attached regime, with $T_t \sim 15$ eV but with significantly higher density: $n_t \sim 4 \times 10^{19}$ m^{-3}, see Figure 2. The total injection time was 30 s (70% of the total flattop time, 8% under Ohmic conditions).

In both experiments, the outer target surface temperatures measured by an infrared camera were around 340-360 K. The surface roughness was $R_a = 30 - 50\mu$m in forward field and $R_a = 1\mu$m in reversed field.

Before the reversed field experiment, the $^{13}CH_4$ injection rates were measured by the in-vessel pressure gauges, by injecting ^{12}C methane into the vacuum. This calibration method is consistent with the one used in TEXTOR ^{13}C experiments, see e.g. [3]. The measured injection rates were 2.3×10^{19} molecules/s for the lower valve (LV) and 1.02×10^{19} molecules/s for the upper valve (UV), exceeding the earlier reports based on baratron signals [1] by factors of 3.8 and 3.4, respectively. Same gas fill pressures and opening voltages of the piezo valves were applied as in the earlier forward field experiment. Therefore, these new measurements of injection rates will be used throughout this paper, for both experiments.

The distribution of locally re-deposited ^{13}C, shown in Figure 3, was measured by nuclear reaction analysis (NRA). The total amount of re-deposited ^{13}C was determined by fitting a surface spline function through the measured NRA points and integrating the fitted function. In forward field, 32% of the ^{13}C injected from the UV and 24% of that injected from the LV was found re-deposited on the surrounding tiles, forming deposition tails in both toroidal directions. A significant fraction (2/5) of the deposition was found on the upstream side of the valves. The deposition pattern also shows a deviation from the magnetic field direction downwards, towards the strike point. This deviation corresponds to the direction of the $\mathbf{E} \times \mathbf{B}$ drift velocity related to the (pre)sheath electric field E_z, see Figure 3.

In reversed field, a factor of 2 lower re-deposition efficiencies are determined from NRA: 18% at the UV and 12% at the LV. During the removal of the tiles part of the hydrogen-rich

layer close to the UV flaked and, therefore, the UV deposition is expected to be slightly underestimated. The deposition in reversed field is very localized around the valves and forms more circular patterns compared to forward field. Transport against the plasma flow appears strongly suppressed, and the fraction of upstream deposition is reduced to 1/5. Close to the valves, the deposition patterns show transport towards the outer scrape-off layer, in line with the reversal of the $\mathbf{E_z} \times \mathbf{B}$ drift. Further downstream, the tails resume the field line direction.

3 Modelling

The SOLPS5.0 code package [4], with the plasma fluid code B2.5 coupled to the Monte Carlo neutrals code Eirene-99 and impurities included in the solution, was used to calculate 2D models of the divertor plasma conditions. The solutions were validated against multiple measurements at the outer target and at the outer midplane, in the two experiments described in this paper. The effect of B_{T} and I_{p} directions on the target conditions was taken into account by fully activating the drifts terms in B2.5. The detailed 3D trajectories of the injected impurities were then calculated with the ERO code [5], using the SOLPS solutions for T_{e}, T_{i}, n_{e}, $v_{\parallel}$ and electric potential V_{p} to describe the plasma background [2]. ERO calculates the formation of the carbon layer, including re-erosion and re-deposition, which is compared to the NRA measurements.

Figures 1 and 2 show the profiles of parallel flux density $\Gamma_{\parallel}$, n_{e}, T_{e} and plasma potential V_{p} along the outer target, as calculated by SOLPS and measured by the flush-mounted Langmuir probes in forward and reversed field, respectively. The probe V_{p} is calculated from the measured values of the floating potential V_{f} and T_{e}: $V_p = V_{\mathrm{f}} + 3T_{\mathrm{e}}$ [6]. A 20% discrepancy in n_{e} between the probe data and SOLPS is due to differences in sound speed models (adiabatic coefficient $\gamma = 3$ in AUG probe data evaluation and $\gamma = 5/3$ in SOLPS).

SOLPS simulations correspond to the measured target conditions in forward field well, with only T_{e} remaining above the measured levels (up to a factor of 2), see Figure 1. Due to low probe biasing voltage, however, the measured T_{t} could be underestimated. Within the last few centimetres from the divertor surface, there is a strong drop in plasma potential in the direction perpendicular to the target, giving a presheath electric field $E_z \sim 1$ V/mm. Around the valve locations, there is an equally large electric field component in the (approximately

radial) direction parallel to the surface: $E_\mathrm{r} = -\mathrm{d}V_\mathrm{p}/\mathrm{d}s \sim 1$ V/mm. Thus, there are two equally significant components of the electric field perpendicular to $\mathbf{B}$, both inducing $v_{\mathbf{E}\times\mathbf{B}} \sim 400$ m/s: (i) parallel to the surface, towards the strike point (E_z) and, (ii) perpendicular to the target, towards the surface (E_r).

The experimentally observed strong increase of n_t with field reversal (by a factor of $\sim$10) is also calculated by SOLPS, see Figure 2. The simulated density profile along the target is, however, more peaked around the strike point than the Langmuir probe data, and the simulated peak T_t remains below 10 eV. At the LV, a reasonable correspondence with probe measurements is obtained in reversed field. At the UV, T_e appears to be overestimated and n_e largely underestimated compared to the Langmuir probe data. At the valve locations, the modelled E_z is similar to forward field, but the modelled E_r is negligible and even pointing in the opposite direction compared to forward field. The modelled increase in V_p radially towards the outer SOL is associated with the modelled T_e profile and, therefore, disagrees with the probe data.

Figure 4 shows the deposition layers calculated with ERO, using the SOLPS solutions for forward and reversed field. Following modelling of TEXTOR experiments, this work uses the assumptions of enhanced chemical re-erosion yield of the re-deposited carbon, $Y_\mathrm{chem} = 15\%$, and small effective hydrocarbon sticking probability, S_eff [7]. However, even small values of S_eff tend to peak the deposition around the exit holes, where a vast majority of impinging particles are hydrocarbons. Laboratory experiments indicate that CH molecules have significantly higher sticking probability than other hydrocarbon species [8]. Therefore, the present modelling assumes S(CH,CH^+)=1 and S=0 for other hydrocarbons, which tends to broaden the patterns compared to a species-independent S_eff. For carbon, sticking probabilities are calculated according to TRIM [5].

In forward field, ERO simulations give re-deposition efficiencies of 30% at the UV and 44% at the LV. Such high deposition rates are caused by ionization within the first few centimetres from the surface, and by the $\mathbf{E_r} \times \mathbf{B}$ drift guiding the ionized particles towards the surface [2]. The calculated $v_{\mathbf{E}\times\mathbf{B}}$ is significant compared to the average velocity right after first reaction to an ionized species $\sim$1400 m/s. The modelled E_r also increases the fraction of upstream deposition: the simulations have 1/3 of the deposition upstream from the valves, which is close

to the measured value (2/5). The observed deviation from the magnetic field line towards the separatrix, arising from the $\mathbf{E_z} \times \mathbf{B}$ drift, is well reproduced. At the UV, very good correspondence with the NRA pattern is obtained, but the deposition at the LV is too peaked. Due to the low energy of neutrals impinging close to the exit hole, sticking of CH is likely to be overestimated. By assuming $S_{\mathrm{eff}} = 0$, better agreement at the LV is obtained, with deposition efficiency reduced to 32%.

In reversed field, ERO simulations give lower re-deposition efficiencies (UV: 24%, LV: 36%), although the ionization lengths are similar to forward field. Because of small E_r, deposition close to the injection is dominated by neutral dissociation products [9], yielding the round pattern in the vicinity of the holes. In accordance with measurements, the modelled deposition tails show smaller deviation from the magnetic field direction compared to forward field, now towards the outer SOL. At the LV, the simulations match the observed small upstream deposition, due to higher plasma friction [9]. The simulated downstream deposition is, however, overestimated, with both ionized and neutral particles impinging on the surface. At the UV, the modelled upstream deposition exceeds the measured values.

The discrepancies in modelled and measured deposition in reversed field could be related to a too strong modelled n_{e} decay along the target, as indicated also by the probe data. With higher n_{e} and, correspondingly, lower T_{e} at the UV the collisionality would be higher, reducing upstream transport. Associated with this are the possible deficiencies in modelled electric potential distribution, which could further explain the indicated overestimation of ions depositing downstream. Finally, the reduced surface roughness in reversed field compared to forward field could also play a role in further reducing the deposition efficiency [3].

4 Conclusions

This paper presented new results from $^{13}CH_4$ injection into an ASDEX Upgrade L-mode plasma under reversed B_{T} and I_{p} configuration, in comparison with an earlier experiment in forward field configuration. The experiments were simulated using the SOLPS5.0 and ERO codes. $\mathbf{E} \times \mathbf{B}$ driven transport was found to play a major role in the transport of carbon at the AUG outer target, resulting in lower re-deposition efficiency for reversed field configuration. The

field reversal was found to directly affect the drift velocity of the impurities and considerably change the target plasma conditions. Inclusion of cross-field drifts in the simulations was found necessary for reproducing the experimental observations.

Acknowledgements

The authors would like to thank Mr. Gilbert de Saint-Aubin for his support in the NRA measurements of the ^{13}C re-deposition. This work, supported by the European Communities under the contract of Association between EURATOM/Tekes, was carried out within the framework of the Task Forces on Plasma Wall Interactions and Integrated Tokamak Modelling of the European Fusion Development Agreement. The views and opinions expressed herein do not necessarily reflect those of the European Commission. The work was partially funded by the Academy of Finland projects No. 121371 and 134930. Part of the computations presented in this document have been made with CSC's computing environment. CSC is the Finnish IT centre for science and is owned by the Ministry of Education.

References

[1] Pugno R *et al*, 2009 *J. Nucl. Mater.* **390-391** 68–71

[2] Aho-Mantila L *et al*, 2010 *Contrib. Plasma Phys.* **50(3-5)** 439–444

[3] Kreter A *et al*, 2008 *Plasma Physics and Controlled Fusion* **50(9)** 095 008

[4] Schneider R *et al*, 2006 *Contrib. Plasma Phys.* **46(1-2)** 3–191

[5] Kirschner A *et al*, 2000 *Nucl. Fusion* **40** 989

[6] Chankin A *et al*, 2007 *Nuclear Fusion* **47(5)** 479

[7] Ding R *et al*, 2010 *Plasma Physics and Controlled Fusion* **52(4)** 045 005

[8] Jacob W, 2005 *J. Nucl. Mat.* **337-339** 839–846

[9] Aho-Mantila L *et al*, 2009 *Phys. Scripta T* **138**. 014019

Figures

Figure 1: Plasma conditions in the outer divertor in forward field, as measured by the Langmuir probes and calculated by SOLPS. The S-coordinate measures the poloidal distance along the target surface. The dashed lines indicate the valve positions. Probe data from the actual ^{13}C discharges is plotted with dots. The diamonds represent data collected during a strike point scan in discharge #22469.

Figure 2: Measured and modelled plasma conditions in the outer divertor in reversed field. Strike point scan was performed in discharge #25881. See caption of Figure 1 for details.

Figure 3: ^{13}C deposition pattern in forward (left) and reversed (right) field, from NRA measurements. The left figure is reproduced from [1], with minor modifications. The solid black lines represent the tile gaps. The dashed black lines indicate the magnetic field direction.

Figure 4: ^{13}C deposition patterns from SOLPS/ERO simulations. See caption of Figure 3.

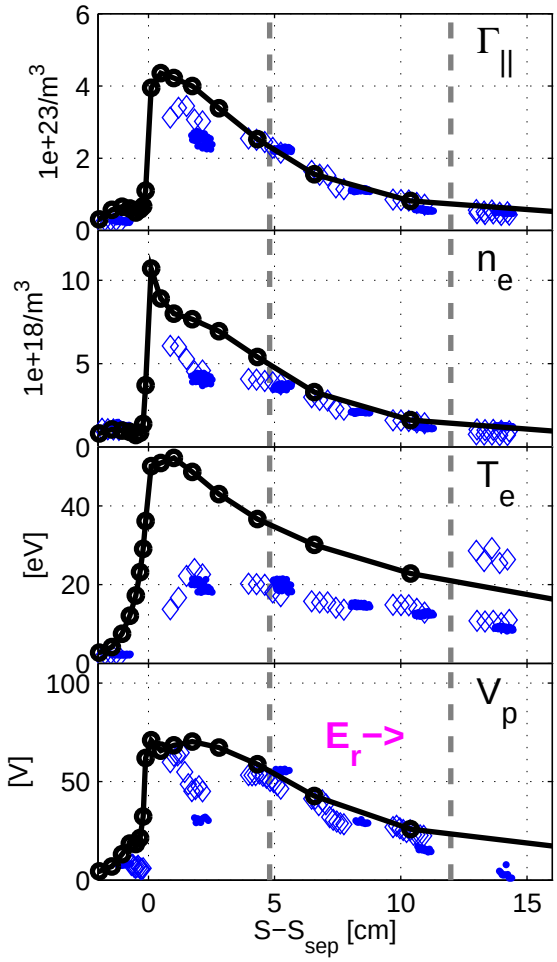

Figure 1

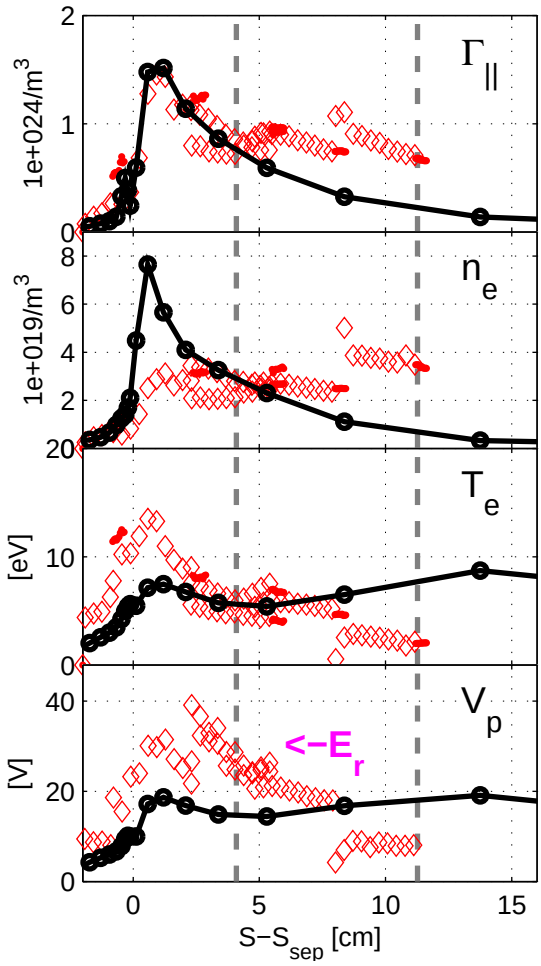

Figure 2

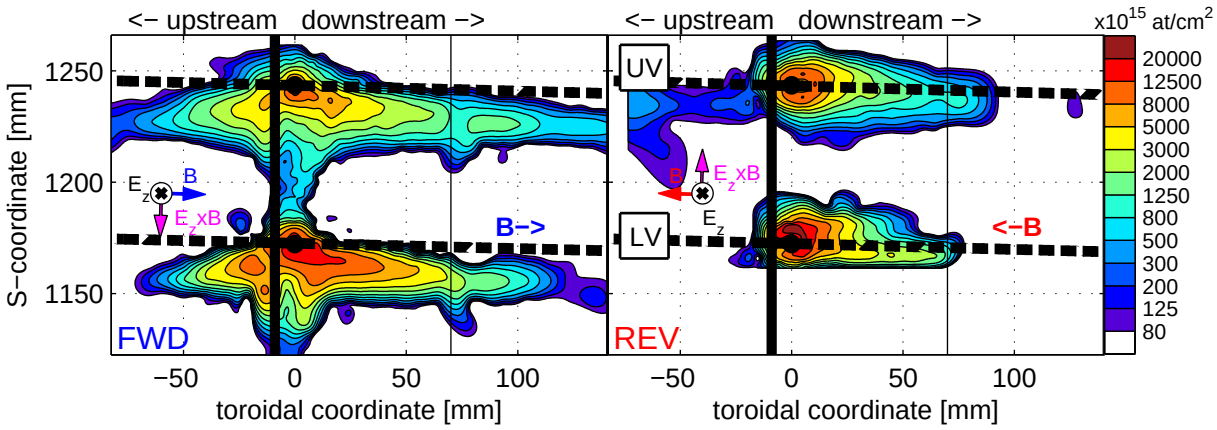
<− upstream downstream −>
<− upstream downstream −>
x10^15 at/cm^2
S−coordinate [mm]
1250
1200
1150
E_z
B
E_z xB
B−>
FWD
UV
LV
E_z xB
B
E_z
<−B
REV
20000
12500
8000
5000
3000
2000
1250
800
500
300
200
125
80
−50
0
50
100
toroidal coordinate [mm]
−50
0
50
100
toroidal coordinate [mm]

Figure 3

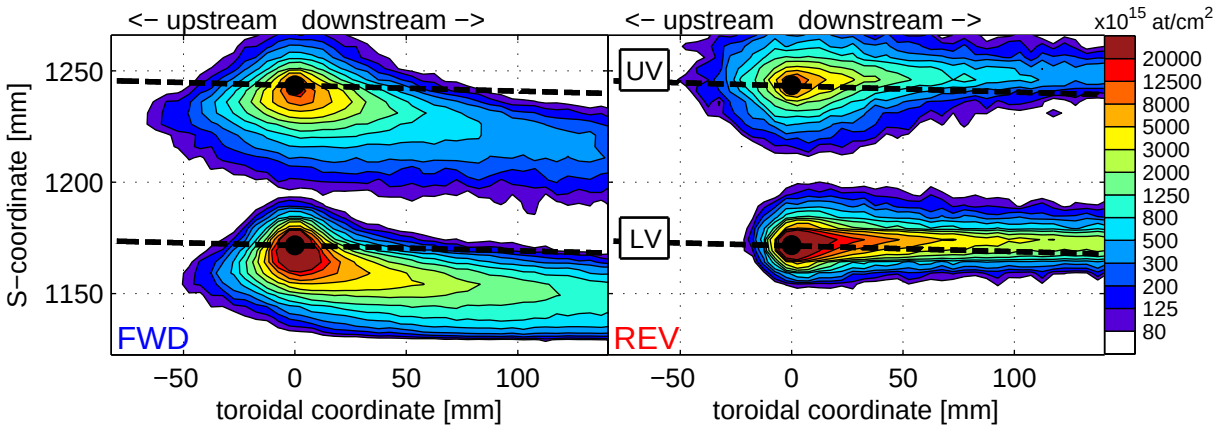
<– upstream downstream –>
<– upstream downstream –>
x10^15 at/cm^2
20000
12500
8000
5000
3000
2000
1250
800
500
300
200
125
80
S–coordinate [mm]
1250
1200
1150
UV
LV
FWD
REV
−50
0
50
100
toroidal coordinate [mm]
−50
0
50
100
toroidal coordinate [mm]

Figure 4